Measurement 218 (2023) 112998

Contents lists available at ScienceDirect

Measurement

journal homepage: www.elsevier.com/locate/measurement

Interpretation of bimodal interference in and optimized operational modal analysis for long-range continuously scanning laser Doppler vibrometer measurements with a beam under white noise excitation

Yuhao Hu [a], Weidong Zhu [b,*], Linfeng Lyu [b], Zhonggang Li [c,*]

[a] Division of Dynamics and Control, School of Astronautics, Harbin Institute of Technology, P.O. Box 137, Harbin 150001, China
[b] Department of Mechanical Engineering, University of Maryland, Baltimore County, 1000 Hilltop Circle, Baltimore, MD 21250, United States
[c] National Demonstration Center for Experimental Mechanics Education, Harbin Institute of Technology, P.O. Box 137, Harbin 150001, China

ARTICLE INFO

Keywords:
Long-range continuously scanning laser Doppler vibrometer system
Bimodal interference
Scanning frequency of mirror
Signal coupling
Optimized operational modal analysis

ABSTRACT

This paper explains the phenomenon of a dominant frequency in the spectrum of a raw response measured by a long-range continuously scanning laser Doppler vibrometer (LCSLDV) system being symmetrically shifted into two sharp peaks. This phenomenon is referred to as bimodal interference in this work, which gradually becomes obvious when the scanning length is greater than 0.5 m. Bimodal interference is significant because it makes natural frequencies unable to be estimated in LCSLDV measurements and this paper analyzes its nature. Natural frequencies and mode shapes of a structure under white noise excitation can be estimated by analysis of its responses measured by the LCSLDV system. The effect of bimodal interference has been ignored in previous LCSLDV and continuously scanning laser Doppler vibrometer (CLSDV) measurement studies, but its appearance makes the value of the dominant frequency not to be accurately identified. By deducing mathematical interpretation of bimodal interference with analysis of incidence and reflection of a continuously scanning laser beam in a tiny time interval and comparing experimental results with 21 groups of different conditions, it is concluded that bimodal interference is caused by signal coupling between the scanning frequency of the mirror and the vibration frequency of the measured structure. There is a positive correlation between the scanning frequency and the magnitude of the symmetric frequency shifts centered at the dominant frequency generated by bimodal interference. In experimental results of LCSLDV measurements with a distance of 60 m, the frequency shift ratio compared to the dominant frequency can be reduced to 0.06% when the scanning frequency is lower than 0.01 Hz. In this case, bimodal interference is not noticeable in the spectrum. The experiment was carried out on a cantilever beam machined based on a prescribed design. Modal parameters of the cantilever beam estimated by white noise excitation were successfully estimated by the LCSLDV system with a distance of 60 m. The maximum difference between the first four natural frequencies of the cantilever beam from the finite element model and the LCSLDV system was 2.97% and the minimum difference was 1.1%.

1. Introduction

As a novel measuring instrument with high coherence and non-contact function, a laser Doppler vibrometer (LDV) has experienced a rapid development [1]. Yeh and Cummins [2] observed for the first-time scattering light of particles in water flow with frequency movement, which proved that the velocity motion of particle flow could be estimated by the laser Doppler translation technology. Huang et al. [3] designed a high-precision calibration system for an LDV to calibrate the reference beam of the LDV. The proposed calibrating method can be utilized in the differential LDV and the spatial filtering vibrometer. Zhou and Long [4] established a mathematic model of an LDV to analyze the Doppler signal of the solid-state surface with the application of the interference fringe model and the principle of light scattering.

When a laser spot is scanned along an arbitrary line, the LDV vibration output is an amplitude-modulated sine wave and operating deflection shapes (ODSs), defined along the scan line, can be established by demodulation [5]. Sriram et al. [6] provided a scanning laser Doppler vibrometer (SLDV) technique based on Chebyshev demodulation for rapid measurement of spatially distributed velocity profiles. Doppler

* Corresponding authors.
E-mail addresses: wzhur@umbc.edu (W. Zhu), lizhonggang@hit.edu.cn (Z. Li).

https://doi.org/10.1016/j.measurement.2023.112998
Received 11 November 2022; Received in revised form 16 April 2023; Accepted 3 May 2023
Available online 11 May 2023

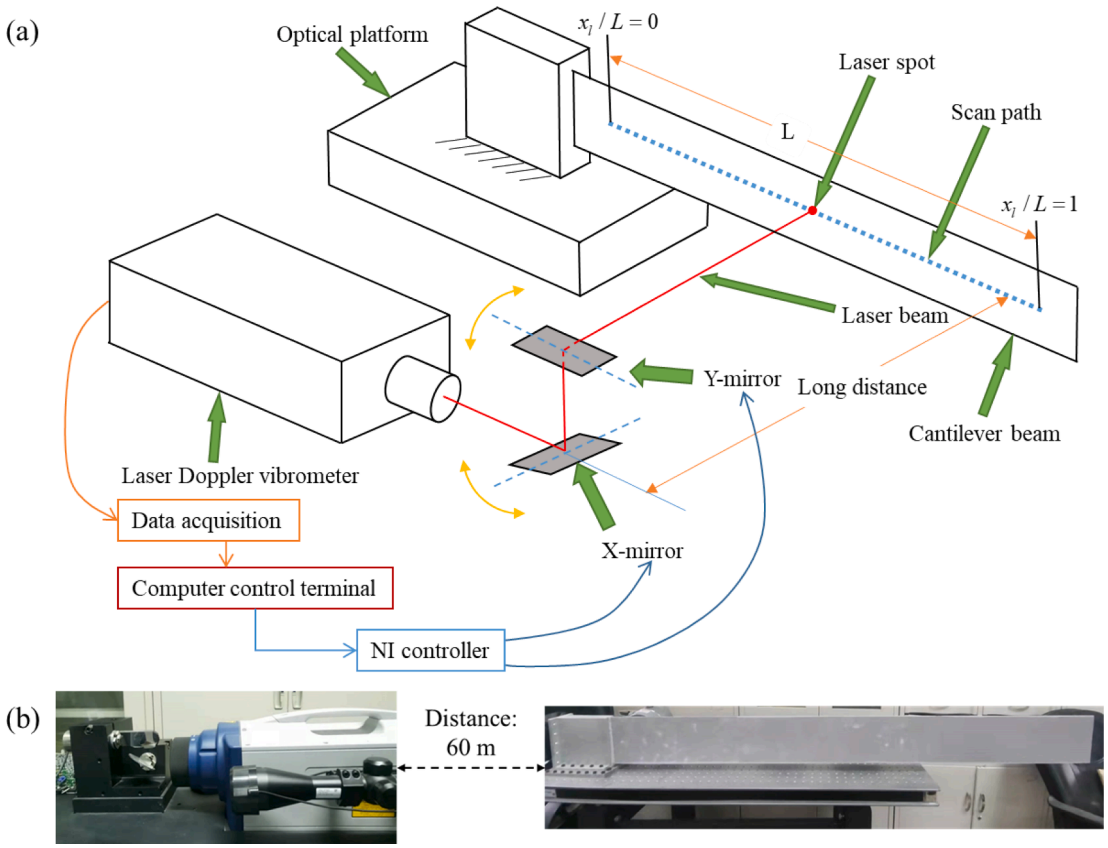

Fig. 1. (a) Schematic of long-range vibration measurement using the LCSLDV system and (b) the diagram of the measuring distance.

signals were processed in the conventional manner using a frequency counter, from which the analog velocity output is post-processed to obtain the velocity profile. Hariharan and Ward [7] described an experiment that unambiguously demonstrated existence of fluctuations in the output of an interferometer due to a frequency shift in the spectrum of a laser beam reflected from the moving mirror.

Many delicate applications of structural vibration measurements require spatially dense measurements, where high spatial resolution and measurements of vibrations of numerous points over the surface are needed. Hence, a continuously scanning laser Doppler vibrometer (CSLDV) is promoted to replace step-by-step scanning that needs the vibrometer to stay at each measuring point for a period of time. A CSLDV provides a non-contact technique for measuring vibration of a structure by continuously moving the laser beam of an LDV along an arbitrary line on the surface of the structure [8]. The advances in vibration measurement performed by a CSLDV augmented the capability of measuring vibrations from a grid of a few hundred measurement points on a structure to a single scan that contains many thousands of points on the structure [9]. Sriram et al. [10] processed a modulated CSLDV velocity output in the spectrum and directly extracted ODSs. Stanbridge et al. [11,12] developed two CSLDV analysis methods, the polynomial method and the demodulation method, to obtain ODSs of a structure under sinusoidal excitation with line, circular and area scans. Maio and Ewins [13] compared step-by-step and continuously scanning methods to introduce a novel approach of continuous scan and multi-tonal excitation waveform. Chen et al. [14] compared the ODSs of beams extracted from a CSLDV system via the polynomial method and the demodulation method. Lyu and Zhu [15] implemented CSLDV measurement on a structure under random excitation and obtained its modal parameters by an improved demodulation method by utilizing an extended filter.

In long-range vibration measurement, one needs to eliminate noise and interference before implementing modal parameter estimation because the environment has considerable effects on the measured response [16]. Interference signals in the long-range LDV measurements used to be divided into speckle noise and ambient noise in physics. The speckle noise is collected by a photodetector and depends on interfering inputs of a random nature mostly related to the characteristics of the measured surface [17]. It inevitably occurs when monochromatic and coherent light is scattered from an optically rough surface. Lv et al. [18] researched the effect of speckle noise of an LDV for long-range measurement and comprehensively discussed statistical properties of dynamic speckles with a combination of theories and experiments. According to experience, adjusting the focal length of LDV helps reduce the speckle noise. Jin and Li [19] provided an algorithm that can eliminate speckle noise for LDV measurements, but their application haven't been verified in LCSLDV measurements. Ambient noise is a form of noise pollution or interference, including water waves, traffic noise, alarms, extraneous speech, electrical noise and so on [20]. One can utilize a smoothing algorithm and wavelet transformation to reduce the influence of ambient noise.

The need for vibration measurements of onshore and offshore wind turbine blades, aeroengine blades in operation and high temperature objects has led to the development of a CSLDV system for long-range vibration measurement. A long-range continuously scanning laser Doppler vibrometer (LCSLDV) system uses the Doppler shift in the frequency of laser to measure velocities of numerous distant points on a scanning path in the direction of the incident laser. Modal parameters extracted from measured responses from a close-range continuously scanning laser Doppler vibrometer (CCSLDV) system and a LCSLDV system can be different. Unlike CCSLDV measurement, LCSLDV measurement is interfered by much noise that reduces signal-to-noise ratios (SNRs) of vibration measurement. Signals with low SNRs contain significant interference in raw responses, resulting in undistinguished

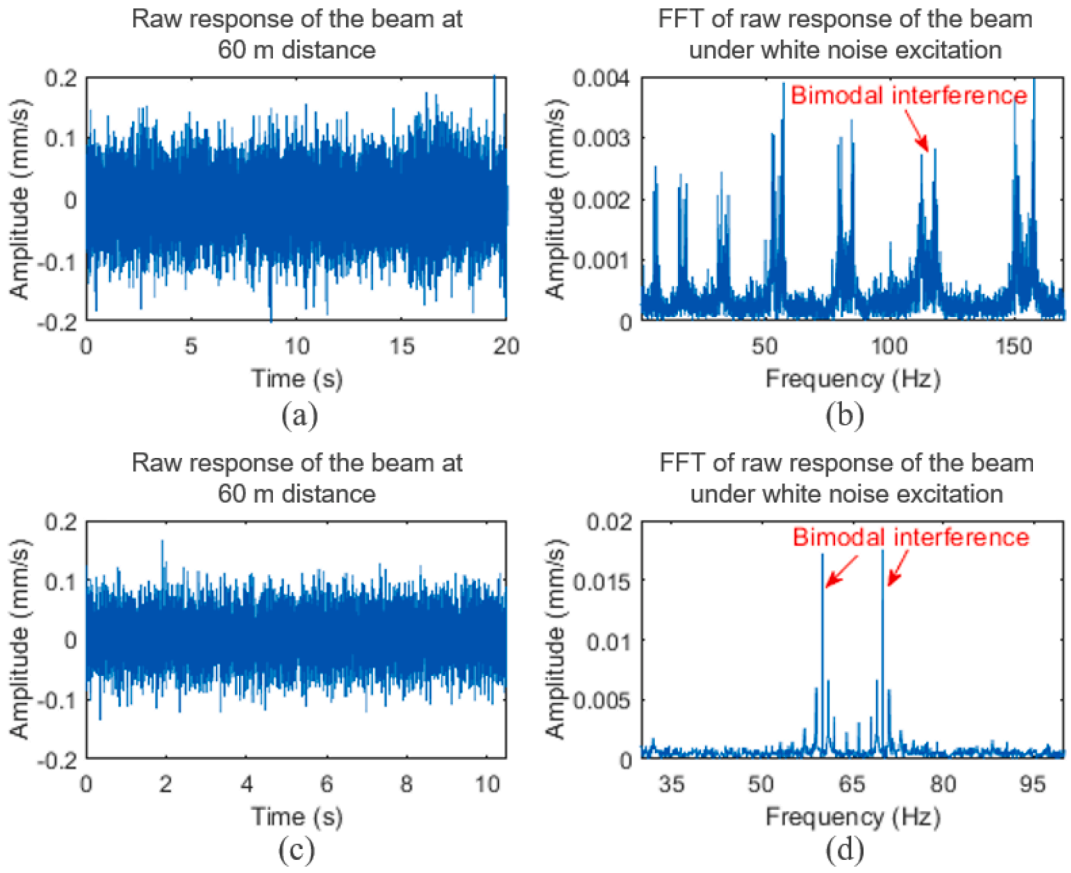

Fig. 2. The (a) time domain and (b) spectrum of bimodal interference with white noise excitation, and (c) and (d) those with a 65 Hz sinusoidal excitation, where FFT in (b) and (d) stands for fast Fourier transform.

dominant frequencies in the spectrum. The value of a dominant frequency is the value of a corresponding natural frequency without non-negligible interference. For instance, in close-range measurement inside a laboratory, the influence of ambient noise on measurement is small. It means that when sinusoidal excitation is applied to a linear time-invariant (LTI) system, the excitation frequency can be perfectly extracted from the response measured by the CCSLDV system. Although the methodology for the LCSLDV system would be similar to that for the CCSLDV system, in LCSLDV measurement outside the laboratory, the authors found that the excitation frequency cannot be obtained from the measured response with original parameter settings of the CCSLDV system in the laboratory. In addition, it is important to note that in past CSLDV measurements, especially LCSLDV measurements, interference that came from the scanning frequency of the mirror used to be ignored.

In this work, it is found that a new coupling interference signal results from scanning in the LCSLDV system. Because the measurement range increases by orders of magnitude in LCSLDV measurement, influence of the rotation of a mirror becomes much more significant. As a result, the dominant frequency that is supposed to center at a value in the spectrum appears in the form of symmetrical frequency shifts. The nature of symmetrical frequency shifts centered at the dominant frequency, which is named bimodal interference in this work, is a signal coupling of the scanning frequency of a mirror in the LCSLDV system and the vibration frequency of the measured structure. The phenomenon of bimodal interference in the spectrum occurs in some papers [16], but the researchers did not concern them because rough natural frequencies estimation was still able to proceed. However, when it comes to the response of a structure with a very small and exactly interested frequency band, such as the structure under sinusoidal excitation, the frequency shifts caused by bimodal interference are non-negligible. What is more, some researches require high accuracy of the spectrum with a wide bandwidth, such as a white noise excitation signal, to implement model updating and other improvements [21]. The apparent symmetrical frequency shifts centered at the dominant frequency make measured modal parameters fuzzy and the value of the dominant frequency not to be estimated in the spectrum.

This paper explains the reason of bimodal interference in LCSLDV measurement and researches the method to eliminate the influence from bimodal interference. A schematic of the LCSLDV system in this work is demonstrated in Fig. 1. A mathematical model was proposed to explain bimodal interference and an improved LCSLDV system with an optimized parameter setting of scanning based on control software was demonstrated. It is the first time that an improved LCSLDV system is developed with the long-range LDV Polytec RSV-150, which employed a longer wavelength and higher laser power than previous instruments. This work is carried out on a cantilever beam that is designed to be sufficiently long so that symmetrical frequency shifts caused by bimodal interference can clearly appear in the spectrum to achieve the experimental accuracy.

The rest of this paper is organized as follows. Interpretation of mathematical models of bimodal interference based on the cantilever beam is presented in Sec. 2.1. Sec. 2.2 demonstrates experimental interpretation of bimodal interference. Sec. 3 explains the signal processing method for the extraction of mode shapes (MSs) of the cantilever beam. The experimental setup of the LCSLDV system is described in Sec. 4.1. Results of optimized operational modal analysis (OMA) of the cantilever beam and comparison of results from the LCSLDV system and the finite element method (FEM) are illustrated in Sec. 4.2. Some conclusions of this study are presented in Sec. 5. The appendix shows results of the traditional modal testing method of the cantilever beam through use of an accelerometer to demonstrate the accuracy of measured natural frequencies from the LCSLDV system.

2. Interpretation of the appearance of bimodal interference

For a LTI system excited by white noise excitation, the values of dominant frequencies in the spectrum should be the same as the values of natural frequencies. For a LTI system excited by a sinusoidal excitation, the value of the dominant frequency in the spectrum should be the same as the frequency of the sinusoidal excitation. When it is a CCSLDV measurement inside the laboratory, the measurement results are consistent with the theorem. However, in LCSLDV measurements, the values of dominant frequencies in the spectrum of the raw response become the values of pairs of peaks symmetrically centered on dominant frequencies, which is the phenomenon of bimodal interference.

The phenomenon of bimodal interference of a LTI system excited by white noise excitation is shown in Fig. 2 **(a)** and **(b)** and that of a LTI system excited by a 65 Hz sinusoidal excitation is shown in Fig. 2 **(c)** and **(d)**. In Fig. 2 **(a)** and **(b)**, one can find that the value of each dominant frequencies, which ought to be equal to natural frequencies, symmetrically shift into pairs of two sharp peaks. In Fig. 2 **(c)** and **(d)**, one can find that the value of the dominant frequency should be 65 Hz, but there are two symmetrically shifted sharp peaks around 65 Hz in the spectrum. These are the obvious phenomenon of bimodal interference. The authors found that modal parameters, especially natural frequencies, cannot be precisely estimated with bimodal interference. The value of the frequency shifts of bimodal interference in a LTI system is an effective standard to judge the accuracy of the LCSLDV system. If the frequency shift of bimodal interference is too obvious in the LCSLDV system, the control parameters of the system must be adjusted, otherwise results from OMA must be inaccurate.

2.1. Interpretation of mathematical models of bimodal interference based on a cantilever beam model

The mathematical interpretation of bimodal interference is based on a long and thin cantilever beam model with respect to the experiment. Assuring that only the vertical displacement of the beam axis of the cantilever beam was considered and both the axial displacement and the rotation of the cross section about the neutral axis were ignored. In addition, the beam satisfied the plane assumption during deformation and assuming there was no deformation caused by shear force. In a periodic LTI system, the time domain can be expressed as

$$T(t) = Csin(\omega t + \varphi) \tag{1}$$

where C is a constant, ω is a frequency and φ is the phase of $T(t)$. The ODS of the cantilever beam can be expressed as

$$\begin{aligned} y(x,t) &= Y(x)T(t) \\ &= C_1 Y(x)sin(\omega t + \varphi) \\ &= V(x_l)sin(\omega_e t) \end{aligned} \tag{2}$$

where x_l is the normalized coordinate position of a laser spot on the surface of the structure along the scan line, ω_e is the excitation frequency and $V(x_l)$ is the ODS of the structure along the scan line. The steady-state response frequency of a LTI structure resulting from sinusoidal excitation is equal to the excitation frequency.

2.1.1. Interpretation of mathematical models in terms of optics

When the LCSLDV system with its X-mirror driven by a triangular input signal measures the steady-state response of a structure under sinusoidal excitation, the velocity response of the structure measured by the system can be expressed as

$$\begin{aligned} v(x_l,t) &= V(x_l)cos(\omega_e t - \delta - \zeta) \\ &= V_I(x_l)cos(\omega_e t) + V_Q(x_l)sin(\omega_e t) \\ &= V(x_l)cos(\delta+\zeta)cos(\omega_e t) + V(x_l)sin(\delta+\zeta)sin(\omega_e t) \end{aligned} \tag{3}$$

where δ is the phase difference between the excitation and X-mirror feedback signal, ζ adjusts amplitudes of the in-phase component $V_I(x_l) = V(x_l)cos(\delta+\zeta)$ and quadrature component $V_Q(x_l) = V(x_l)sin(\delta+\zeta)$ of the ODSs for the condition of sinusoidal excitation.

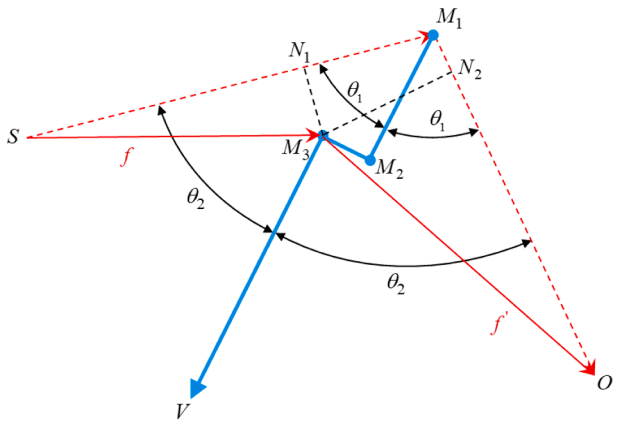

Fig. 3. The diagram of the scanning laser Doppler.

The diagram of laser incidence and reflection under continuous scanning is shown in Fig. 3. f is the emission frequency of the laser beam, f' is the reflected frequency of the laser beam, c is the speed of laser spot, S is the position of the light source of the laser and O is the location of the light wave receiver. In a tiny time interval Δt, a point on the cantilever beam vibrates from the position M_1 to the position M_2 while a laser spot scans from the position M_2 to the position M_3 on the cantilever beam at the same time. One needs to note that M_2 and M_1 are two positions of the same point on the surface of the cantilever beam at different times. M_1 is the position of this point before the time interval Δt and M_2 is that after the time interval Δt. SM_1 and M_1O are the incident and reflected light paths of laser before Δt. SM_3 and M_3O are the incident and reflected light paths of laser after Δt. θ_1 and θ_2 are the angles between the vibration direction of the points M_3 and M_1 on the cantilever beam and the scanning path, respectively. One should pay attention that there is a time interval Δt between M_2 and M_3, and the angle of the laser beam changes a little. Hence, M_1M_2 and M_3V are not strictly parallel. Supposing that m is the number of light wave periods in the scanning path from the light source to the receiver, in this laser path, the change of m is [22]

$$-\Delta m = \frac{M_3N_1}{\lambda} + \frac{M_3N_2}{\lambda'} \tag{4}$$

where M_3N_1 and M_3N_2 are perpendicular to the original optical path, and λ and λ' are the wavelengths of the laser beam before and after reflection, respectively. Because of the tiny time interval Δt, the velocity v_1 of the laser spot and the vibration velocity v_2 of the cantilever beam are considered to be uniform. Hence, $M_1M_2 = v_2\Delta t$, $M_2M_3 = v_1\Delta t$. Eq. (4) can be expressed as

$$-\Delta m = \frac{v_2\Delta t cos\theta_2}{\lambda} + \frac{v_1\Delta t cos\theta_2}{\lambda'} \tag{5}$$

Because

$$f\lambda = f'\lambda' = c \tag{6}$$

and

$$\Delta f = f' - f = -\frac{dm}{dt} \tag{7}$$

where Δf is the differential frequency of the laser beam. Based on Eqs. (5) to (7), one can obtain

$$\Delta f(v_1, v_2) = \frac{v_1 f cos\theta_2}{c} + \frac{v_2 f' cos\theta_2}{c} \tag{8}$$

Because the laser Doppler vibrometer used in the experiment emits a wavelength of 1550 nm, both the order of f and f' are 10^{14}. The first four

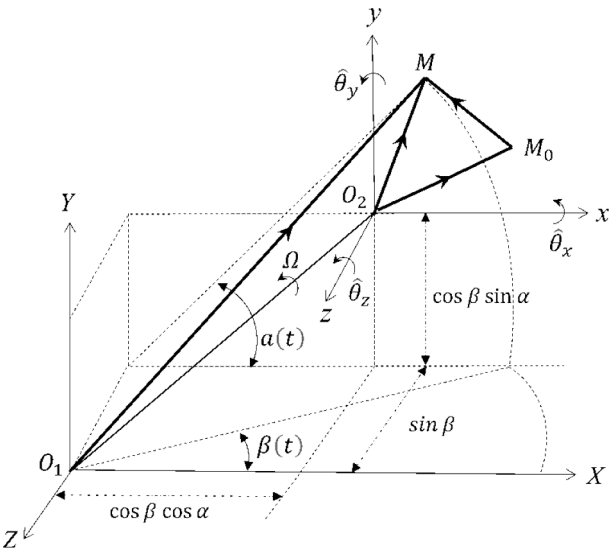

Fig. 4. Orientation of the laser beam O_1M defined by angles $\alpha(t)$ and $\beta(t)$.

natural frequencies of the cantilever beam measured in this experiment are less than 100 Hz so the variation among f and f' is very small. Compared with difference between v_1 and v_2, the difference between f and f' can be ignored. Therefore, f and f' can be assumed to be approximately equal. Hence, Eq. (8) can be approximated as

$$\begin{aligned}\Delta f(v_1, v_2) &= \frac{f}{c}(v_1\cos\theta_2 + v_2\cos\theta_2) \\ &= \Delta f_1 + \Delta f_2\end{aligned} \tag{9}$$

where Δf_1 is the vibrational frequency of the cantilever beam and Δf_2 is the frequency caused by the scanning. Eq. (9) demonstrates that scanning frequency is capable of affecting the reflected frequency of the laser beam. In addition, when θ_2 is close to zero, the contribution of the velocity v_1 of the laser spot, which is relative to the scanning frequency, is much smaller than that of the vibration velocity v_2. Therefore, Δf_2 will be very small and this is the reason why there is a critical measurement length of obvious appearance of bimodal interference, which is demonstrated in Fig. 9.

2.1.2. Interpretation of mathematical models in terms of dynamics

The following is the derivation of the general velocity measured at a point by a laser Doppler vibrometer. With reference to Fig. 4, a unit vector O_1M describes the direction of the incident laser beam. O_1M, which is orientated by the angles $\alpha(t)$ and $\beta(t)$, is given by [1]

$$\overrightarrow{O_1M} = [cos\beta(t)cos\alpha(t)]\hat{x} + [cos\beta(t)sin\alpha(t)]\hat{y} - [sin\beta(t)]\hat{z} \tag{10}$$

where $\overrightarrow{O_1M}$ is equal to $\hat{x}$ at the beginning, first rotates an angle $\beta(t)$ around $\hat{y}$, then rotates an angle $\alpha(t)$ around $\hat{z}$. O_1-XYZ is the global coordinate and O_2-xyz is the translating reference coordinate. The general velocity measured by a laser beam, whilst undergoing an arbitrary vibration, can be derived:

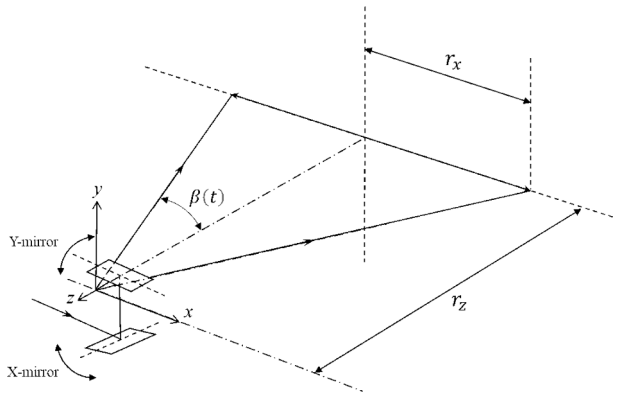

Fig. 5. Straight-line scanning with X-mirror rotating only.

$$\begin{aligned}v(t) = {} & \cos\beta(t)\cos\alpha(t)\left[\dot{x} + \left(\dot{\theta}_x + \Omega\right)y - \left(\dot{\theta}_y - \Omega\theta_x\right)z\right] \\ & + \cos\beta(t)\sin\alpha(t)\left[\dot{y} - \left(\dot{\theta}_z + \Omega\right)x + \left(\dot{\theta}_x + \Omega\theta_y\right)z\right] \\ & - \sin\beta(t)\left[\dot{z} - \left(\dot{\theta}_z + \Omega\theta_y\right)y + \left(\dot{\theta}_y - \Omega\theta_x\right)x\right] \\ & - (y_0\sin\beta(t) + z_0\cos\beta(t)\sin\alpha(t))\left(\dot{\theta}_x + \Omega\theta_y\right) \\ & + (z_0\cos\beta(t)\cos\alpha(t) + x_0\sin\beta(t))\left(\dot{\theta}_y - \Omega\theta_x\right) \\ & + (x_0\cos\beta(t)\sin\alpha - y_0\cos\beta(t)\cos\alpha(t))\left(\dot{\theta}_z + \Omega\right)\end{aligned} \tag{11}$$

where x, y, z and $\dot{x}$, $\dot{y}$, $\dot{z}$ are translational vibration displacements and velocities of the translating reference origin O_2, θ_x, θ_y, θ_z and $\dot{\theta}_x$, $\dot{\theta}_y$, $\dot{\theta}_z$ are the angular vibration displacements and velocities of the shaft around the x, y, z axes, Ω is the rotation speed of the axial O_1O_2 and (x_0, y_0, z_0) is the position of an arbitrary origin point on the scanning path of the laser beam.

The instantaneous laser spot M with the deformed position is identified by the position vector O_2M in the translating reference coordinate, and the instantaneous laser spot M_0 with the undeformed position is defined by the position vector O_2M_0. One can get

$$\overrightarrow{O_1M} = \overrightarrow{O_1O_2} + \overrightarrow{O_2M} = \overrightarrow{O_1O_2} + \overrightarrow{O_2M_0} + \overrightarrow{M_0M} \tag{12}$$

where $\overrightarrow{O_1M}$ represents the position of M relative to the global coordinate O_1-XYZ, O_1O_2 represents the instantaneous position of the translating reference coordinate O_2-xyz and $\overrightarrow{M_0M}$ is the deformation. The difference of $\overrightarrow{M_0M}$ represents the deformation vibration velocity of M according to cross-section flexibility. The velocity measured by the laser Doppler vibrometer is $v(t)$ in a periodical LTI system, which can be written as [23]

$$\begin{aligned}v(t) = {} & \cos\beta\cos\alpha\left[\dot{x}_r(P_0) + \dot{x}_f(P)\right] + \cos\beta\sin\alpha\left[\dot{y}_r(P_0) + \dot{y}_f(P)\right] \\ & - \sin\beta\left[\dot{z}_r(P_0) + \dot{z}_f(P)\right]\end{aligned} \tag{13}$$

where $\dot{x}_r(P_0)$, $\dot{y}_r(P_0)$ and $\dot{z}_r(P_0)$ are components of the vibration velocity in the x, y, z directions caused by cross-section flexibility of a rigid body, $\dot{x}_f(P)$, $\dot{y}_f(P)$ and $\dot{z}_f(P)$ are components of the vibration velocity in the x, y, z directions caused by cross-section flexibility.

For a straight-line scanning measurement, the scanning path on the surface of the measured structure is just one dimension, as shown in Fig. 5. Hence, $\alpha(t)$ is equal to zero because the scanning path is parallel to the x-z plane. The origin of the coordinate xyz is out of the surface of the Y-mirror because the laser spot reflected by the X-mirror is non-stationary on the Y-mirror. The velocity of the laser spot measured

Table 1
The relation between the scanning frequency and frequency shift of bimodal interference.

Test	ω_{sc}	f_b	e	k
1	2 Hz	8.0476 Hz	12.38%	4.0238
2	1 Hz	5 Hz	7.69%	5
3	0.5 Hz	2 Hz	3.08%	4
4	0.1 Hz	0.4 Hz	0.62%	4
5	0.05 Hz	0.2 Hz	0.31%	4
6	0.01 Hz	0.04 Hz	0.06%	4

during a straight-line scanning can be obtained through rearranging Eq. (13) and submitting $\alpha(t) = 0$ into it:

$$v(t) = \cos(\beta(t))\left[\dot{x}_f(P)\right] - \sin(\beta(t))\left[\dot{z}_f(P)\right] \tag{14}$$

For uniform motion which is periodically repeated in a straight line, the angle $\beta(t)$ is expressed as a normalized trigonometric function with coefficients k and the scanning frequency ω_{sc} of the X-mirror. The coefficient k describes the value of the frequency shift caused by bimodal interference. According to the results of experiments, k is positively correlated to the scanning frequency, as shown in Eq. (21) and Table 1. In order to match the point-to-point analysis in Fig. 3, the periodical LTI system is decomposed into a discrete LTI system in the following analysis. Therefore, one can obtain the discrete expression of $\beta(t_n)$ in the time domain, which is given by

$$\begin{aligned} \cos(\beta(t_n)) &= \frac{r_x}{r_z} cos(k\omega_{sc}t_n), \\ \sin(\beta(t_n)) &= \frac{r_x}{r_z} sin(k\omega_{sc}t_n), \\ n &= 1,\ 2,\ 3,\ \cdots,\ N \end{aligned} \tag{15}$$

where r_x is the half of the scanning distance, r_z is the vertical distance between the coordinate xyz and the scanning path, t_n is the discrete time and n is the number of virtual measurement points got from the LCSLDV system. By submitting Eq. (15) into Eq. (14), $v(t_n)$ can be rearranged as

$$v(t_n) = \frac{r_x}{r_z} cos(k\omega_{sc}t_n)\left[\dot{x}_f(P)\right] - \frac{r_x}{r_z} sin(k\omega_{sc}t_n)\left[\dot{z}_f(P)\right] \tag{16}$$

When one only considers the vibration in the x direction, the term $\dot{z}_f(P)$ can be ignored. By considering the variables of the phases δ and ζ in Eq. (3), the formula of the excitation generated from a sinusoidal frequency signal can be expressed as

$$f(t_n) = A_0 cos(\omega_e t_n - \delta - \zeta) \tag{17}$$

where $f(t_n)$ is the excitation signal and A_0 is a constant. Hence, through referring to Eq. (3), the vibration velocity component $\dot{x}_f(P)$ in the x direction caused by cross-section flexibility can be written as

$$\dot{x}_f(P) = A_1 V(x_l) cos(\omega_e t_n - \delta - \zeta) \tag{18}$$

Submitting Eq. (18) into Eq. (16) and ignoring the irrelevant components, one can obtain the velocity $v(x_l, t_n)$ measured by the laser Doppler vibrometer in the x direction:

$$\begin{aligned} v(x_l, t_n) &= A_1 V(x_l) \frac{r_x}{r_z} cos(k\omega_{sc}t_n) cos(\omega_e t_n - \delta - \zeta) \\ &= AV(x_l) cos(\omega_e t_n - \delta - \zeta) cos(k\omega_{sc}t_n) \end{aligned} \tag{19}$$

where $A = A_1 \frac{r_x}{r_z}$. By rearranging Eq. (19) with a trigonometric identity, the velocity response of the structure measured by the LCSLDV system, which explains the frequency Δf_1 and Δf_2 in Eq. (9), can be expressed as

$$\begin{aligned} v(x_l, t_n) &= V'(x_l) cos[(\omega_e \pm k\omega_{sc})t_n - \delta - \zeta] \\ &= V'(x_l) cos(\delta + \zeta) cos[(\omega_e \pm k\omega_{sc})t_n] + V'(x_l) sin(\delta + \zeta) sin[(\omega_e \pm k\omega_{sc})t_n] \\ &= V'_I(x_l) cos[(\omega_e \pm k\omega_{sc})t_n] + V'_Q(x_l) sin[(\omega_e \pm k\omega_{sc})t_n], \\ n &= 1,\ 2,\ 3,\ \cdots,\ N \end{aligned} \tag{20}$$

where $V'(x_l) = AV(x_l)$, $V'_I(x_l) = V'(x_l) cos(\delta + \zeta)$ and $V'_Q(x_l) = V'(x_l) sin(\delta + \zeta)$ are the in-phase and quadrature components of the ODSs with the continuously scanning measurement of the structure, respectively.

After the Fourier transform, δ and ζ do not cause frequency shift interference in the spectrum while the frequency $\omega_e \pm k\omega_{sc}$ of the in-phase and quadrature components will form a double peak appearance in the spectrum, which is the frequency shift of bimodal interference.

2.2. Experimental interpretation of bimodal interference

In LCSLDV measurement, the appearance of bimodal interference caused by the signal coupling of the scanning frequency ω_{sc} and the sinusoidal excitation frequency ω_e is sometimes very obvious. There were four types of experiments to illustrate the influence factor of bimodal interference. In order to reduce and compare the effects of ambient noise, the following experiment was carried out in a very quiet environment. In addition, one should pay attention that the speckle noise is one of the significant reasons that leads to the sidebands in the spectrum during OMA [8].

The first type of comparative experiments was implemented on the LCSLDV system with 0.1 Hz, 0.5 Hz and 1 Hz scanning frequencies at distances of 20 m, 40 m and 60 m on the measured structure under a 65 Hz sinusoidal excitation, respectively. In addition, the sampling frequency in this type was 4 Hz and the scanning length in this type was around 1.45 m. As shown in Fig. 6, when the scanning frequency was 0.1 Hz, the frequency shift caused by bimodal interference was the same when the measuring distance was 20 m, 40 m and 60 m. In addition, when the scanning frequencies was 0.5 Hz and 1 Hz, the frequency shift caused by bimodal interference was also unchanged. Therefore, the difference of the distance between the LCSLDV system and the structure has no noticeable effect on the elimination and decrease of bimodal interference in the spectrum of the raw response. In addition, there is no aliasing in the LCSLDV system because the change of the sampling frequency has no noticeable effect on the frequency in the spectrum of the raw response after the fast Fourier transform (FFT).

The second type of comparative experiments was implemented on the LCSLDV system with 1 k Hz, 4 k Hz, 8 k Hz, 12 k Hz, 16 k Hz and 20 k Hz sampling frequencies at the same distance of 60 m on the measured structure under a 65 Hz sinusoidal excitation, respectively. In addition, the scanning frequency in this type was 1 Hz and the scanning length in this type was around 1.45 m. As shown in Fig. 7, the difference of the sampling frequency of the LCSLDV system has no noticeable effect on the elimination and decrease of bimodal interference in the spectrum of raw response after the FFT.

The third type of comparative experiments was implemented on the LCSLDV system with 2 Hz, 1 Hz, 0. 5 Hz, 0.1 Hz, 0.05 Hz and 0.01 Hz scanning frequencies at the same distance of 60 m on the measured structure under a 65 Hz sinusoidal excitation, respectively. In addition, the sampling frequency in this type was 4 k Hz and the scanning length in this type was around 1.45 m. As shown in Fig. 8, with the decrease of scanning frequency, the interval between the two peaks decreases. Finally, only when the distinguishability was amplified, the two peaks of bimodal interference would appear in the spectrum. One can know that the difference of the sampling frequency of the LCSLDV system has significant effect on the elimination of bimodal interference in the spectrum of the raw response after the FFT. The relation between the

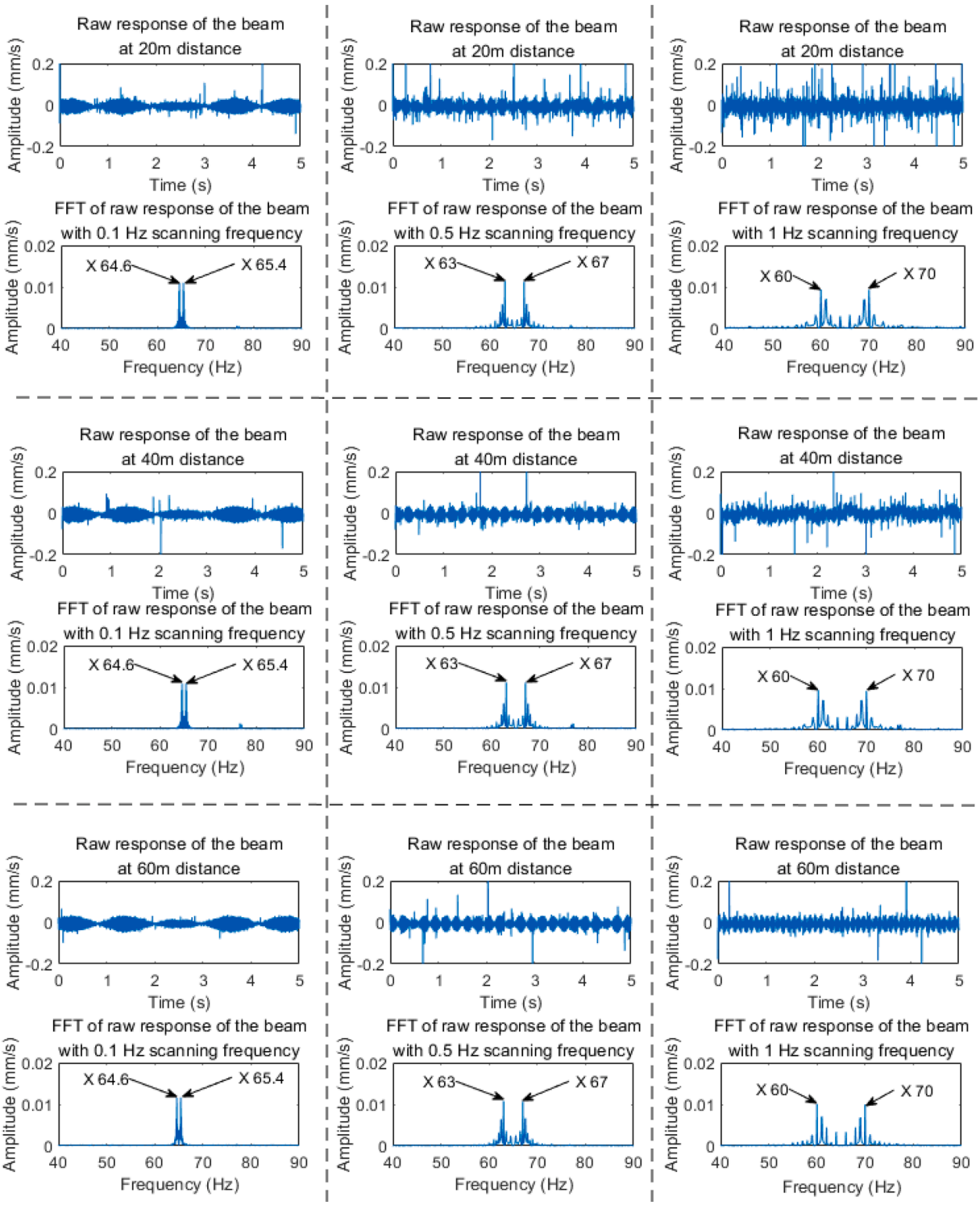

Fig. 6. Time domains of responses and their spectra with different measuring distances.

scanning frequency and the frequency shift of bimodal interference was shown in Table 1 and the error rate e was the ratio of the frequency shift of bimodal interference and the dominant frequency. Moreover, k in Eq. (20) in this experiment was equal to the quotient of the frequency shift f_b of bimodal interference and the scanning frequency ω_{sc}, which is

$$k = \frac{f_b}{\omega_{sc}} \tag{21}$$

It is obvious that the frequency shift of bimodal interference is positively correlated with the scanning frequency of the mirror.

Last but not least, many LCSLDV and CSLDV measurements did not observe bimodal interference phenomenon because the scanning lengths in these experiments were insufficiently long. After more than 200 experiments, the researchers found that the appearance of bimodal interference was relative to the scanning length in the LCSLDV measurements. A main peak is in the form of a dominant frequency that is supposed to be. The changes of the main peak and bimodal interference with the increase of the scanning length were shown in Fig. 9.

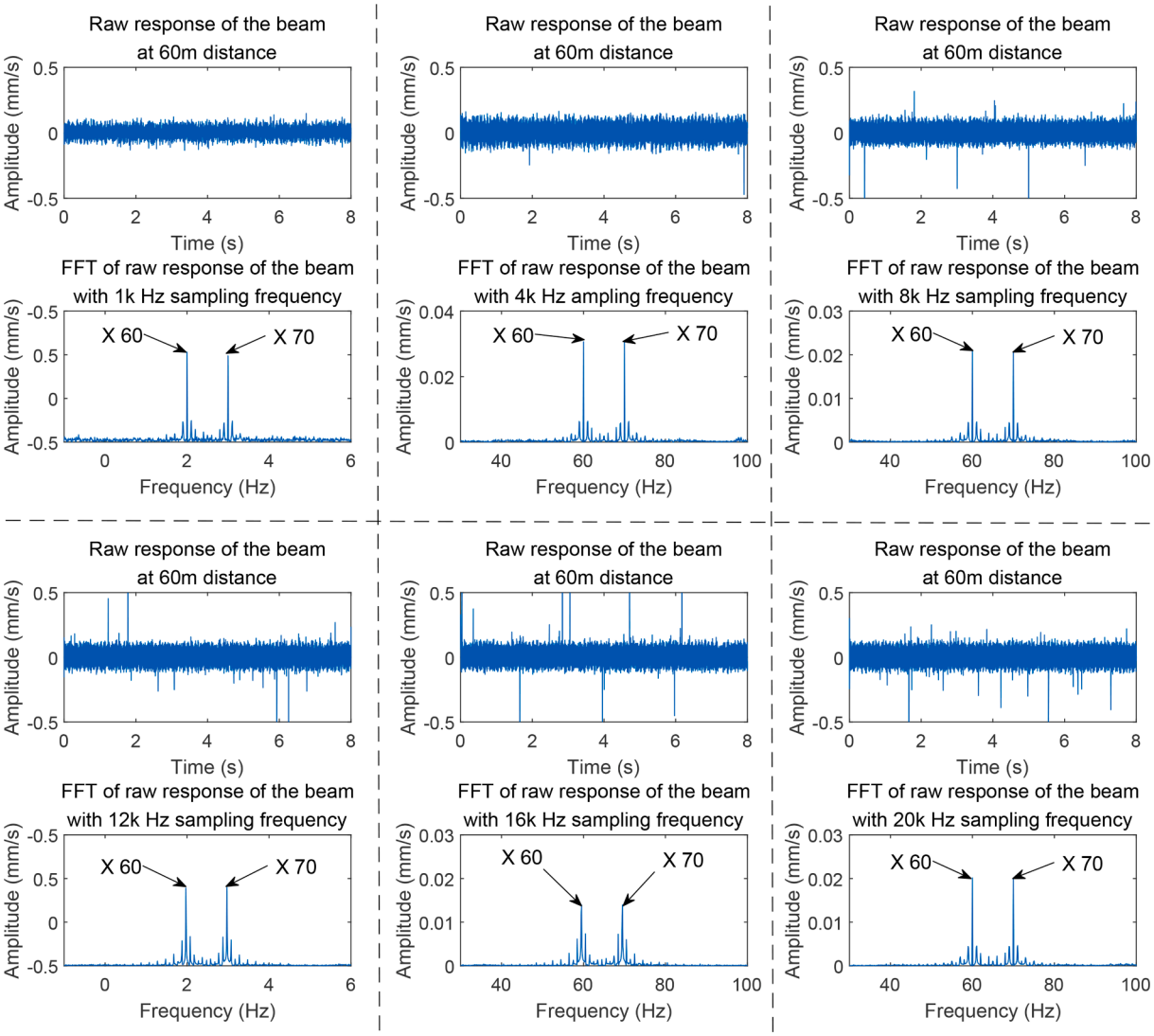

Fig. 7. Time domain responses and their spectra with different sampling frequencies.

Readers only need to pay attention to the relationship between bimodal interference and the main peak in the term of the scanning length. The amplitude of bimodal interference was equal to that of the main peak when the scanning length was around 0.5 m. One can find that the main peak relatively decreases and bimodal interference gradually rises with the increment of the scanning length. Finally, bimodal interference swamped the main peak. When the scanning length in this work is larger than 0.5 m, bimodal interference becomes obvious and cannot be ignored. According to experimental results, until now, there is no observed obvious tendency of the critical scanning length with different measurement distances, sampling frequencies and scanning frequencies in this work. What is more, one should note that it is only credible to compare bimodal interference with the main peak in the same type of experiments because the external interference is different in each experiment. The external interference includes the reliability of the instrument interface, ambient noise, the frequency of the power supply and even vibration experiments in the surrounding laboratory. In addition, according to experimental results, bimodal interference only obviously appears in LCSLDV measurements and it can be observed when the measuring distance is over 10 m.

Note that there were more than 200 effective measurements to support the relationship between bimodal interference and the variables. In order to better illustrate the trend of the relationship, the displayed measurement results are representative results.

3. Demodulation method for extraction of MSs

The OMA method used in this experiment is the demodulation method [5,15]. The demodulation method was developed for extraction of ODSs with a structure under sinusoidal excitation. This method can be improved by signal processing for extraction of MSs under white noise excitation. Before implementing the demodulation method, a band-pass filter with a narrow bandwidth is performed on the raw response. One should note that the center frequency of the narrow bandwidth is one of the natural frequencies of the measured structure. In addition, the purpose of the narrow bandwidth of the band-pass filter is making the processed raw responses to be similar to the responses measured from a structure under sinusoidal excitation. The bandwidth of the band-pass filter used in this work is $\pm$ 0.01 Hz centered at the interested natural frequency. After this signal processing, the demodulation method can be utilized for OMA with white noise excitation.

For the condition that the structure is under sinusoidal or narrow band excitation, $V(x_l)$ in Eq. (3) is an ODS. However, for the condition that the structure is under wide band excitation such as white noise excitation, a MS can be extracted from the demodulation method. Therefore, $V(x_l)$ in Eq. (3) can be more accurately expressed as the MS, which is noted as $\boldsymbol{\phi}$.

The standard matrix form of the forced vibration equation for a LTI system with multiple degrees of freedom is

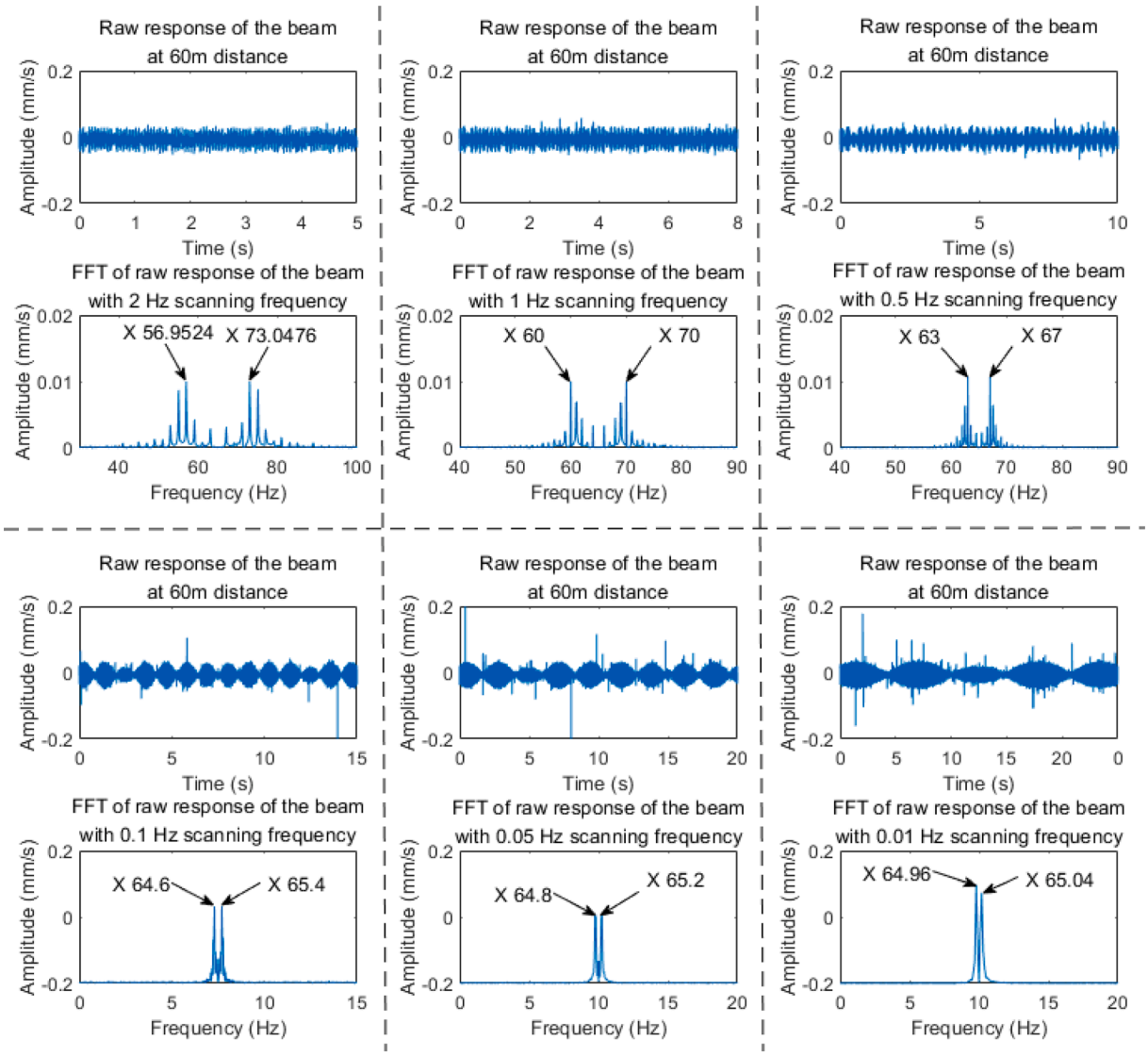

Fig. 8. Time domains responses and their spectra with different scanning frequencies.

$$\boldsymbol{M}\ddot{\boldsymbol{x}}(t)+\boldsymbol{C}\dot{\boldsymbol{x}}(t)+\boldsymbol{K}\boldsymbol{x}(t)=\boldsymbol{F}(t) \tag{22}$$

where $\boldsymbol{M}$ is the mass matrix, $\boldsymbol{C}$ is the damping matrix, $\boldsymbol{K}$ is the stiffness matrix, $\boldsymbol{F}(t)$ is a vector of white noise excitation and $\boldsymbol{x}(t)$ is a vector of displacement response. In addition, $\boldsymbol{x}(t)$ can be written in the modal expansion form

$$\boldsymbol{x}(t)=\boldsymbol{\phi}\boldsymbol{q}(t)=\sum_{r=1}^{k}\boldsymbol{\phi}^{r}\boldsymbol{q}(t) \tag{23}$$

where $\boldsymbol{q}(t)$ is the generalized coordinate vector, $\boldsymbol{\phi}$ is the MS vector and k is the number of modes to be retained.

After change of analog signals to digital signals in experiments, the velocity responses extracted from the LCSLDV system are transformed into discrete time series t_n. As described in Sec. 2.1, the velocity response of the structure measured by the system along a straight scan line is $V(x_l, t_n)$. In order to obtain MSs, the demodulation method is utilized to multiply and filter the velocity response $V(x_l, t_n)$. The band-pass filter is applied to the velocity response $V(x_l, t_n)$ to remove the response outside the interested natural frequency ω_r. The filtered velocity response is noted as $V_f(x_l, t_n)$. After the band-pass filter, $V_f(x_l, t_n)$ only includes the modal parameters of the rth mode. Hence, $V^{'}(x_l)$ in Eq. (3) without bimodal interference contains modal information of $\boldsymbol{\phi}^{r}(x_l)$. For the velocity responses extracted from the LCSLDV system, $V_f(x_l, t_n)$ can also be expressed as

$$\begin{aligned} V_f(x_l,t_n) &= \boldsymbol{\phi}^{r}(x_l)cos(\omega_r t_n-\delta-\zeta) \\ &= \boldsymbol{\phi}_I^{r}(x_l)cos(\omega_r t_n)+\boldsymbol{\phi}_Q^{r}(x_l)sin(\omega_r t_n) \end{aligned} \tag{24}$$

where $\boldsymbol{\phi}_I^{r}(x_l)=\boldsymbol{\phi}^{r}(x_l)cos(\delta)$ is the in-phase component of the rth MS and $\boldsymbol{\phi}_Q^{r}(x_l)=\boldsymbol{\phi}^{r}(x_l)sin(\delta)$ is the quadrature component of the rth MS. Then, $V_f(x_l, t_n)$ in Eq. (24) is multiplied by $cos(\omega_r t_n)$ and $sin(\omega_r t_n)$, which gives

$$\begin{aligned} V_f(x_l,t_n)cos(\omega_r t_n) &= \boldsymbol{\phi}_I^{r}(x_l)cos(\omega_r t_n)cos(\omega_r t_n)+\boldsymbol{\phi}_Q^{r}(x_l)sin(\omega_r t_n)cos(\omega_r t_n) \\ &= \frac{1}{2}\boldsymbol{\phi}_I^{r}(x_l)+\frac{1}{2}\boldsymbol{\phi}_I^{r}(x_l)cos(2\omega_r t_n)+\frac{1}{2}\boldsymbol{\phi}_Q^{r}(x_l)sin(2\omega_r t_n) \end{aligned} \tag{25}$$

$$\begin{aligned} V_f(x_l,t_n)sin(\omega_r t_n) &= \boldsymbol{\phi}_I^{r}(x_l)cos(\omega_r t_n)sin(\omega_r t_n)+\boldsymbol{\phi}_Q^{r}(x_l)sin(\omega_r t_n)sin(\omega_r t_n) \\ &= \frac{1}{2}\boldsymbol{\phi}_Q^{r}(x_l)+\frac{1}{2}\boldsymbol{\phi}_I^{r}(x_l)sin(2\omega_r t_n)-\frac{1}{2}\boldsymbol{\phi}_Q^{r}(x_l)cos(2\omega_r t_n) \end{aligned} \tag{26}$$

respectively. Second and third terms on the second lines of Eq. (25) and Eq. (26) can be eliminated by applying a low-pass filter to $\boldsymbol{\phi}_I^{r}(x_l)\cos(2\omega_r t_n)$ and $\boldsymbol{\phi}_Q^{r}(x_l)\sin(2\omega_r t_n)$ to yield $\frac{1}{2}\boldsymbol{\phi}_I^{r}(x_l)$ and $\frac{1}{2}\boldsymbol{\phi}_Q^{r}(x_l)$,

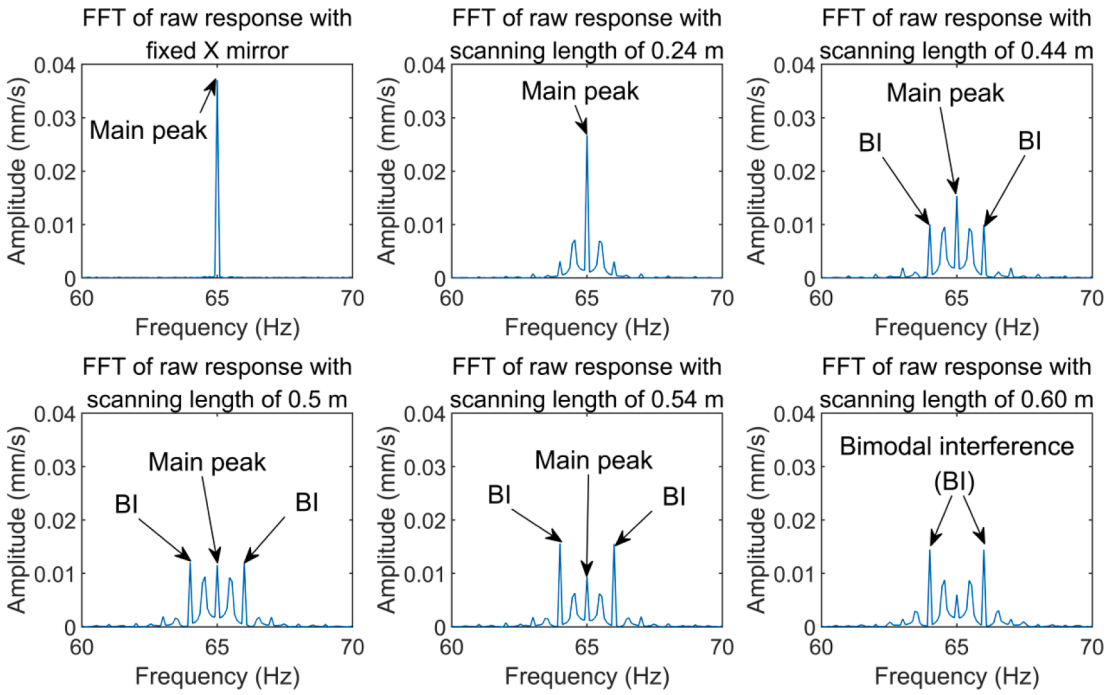

Fig. 9. Changes of the main peak and bimodal interference with the increase of the scanning length.

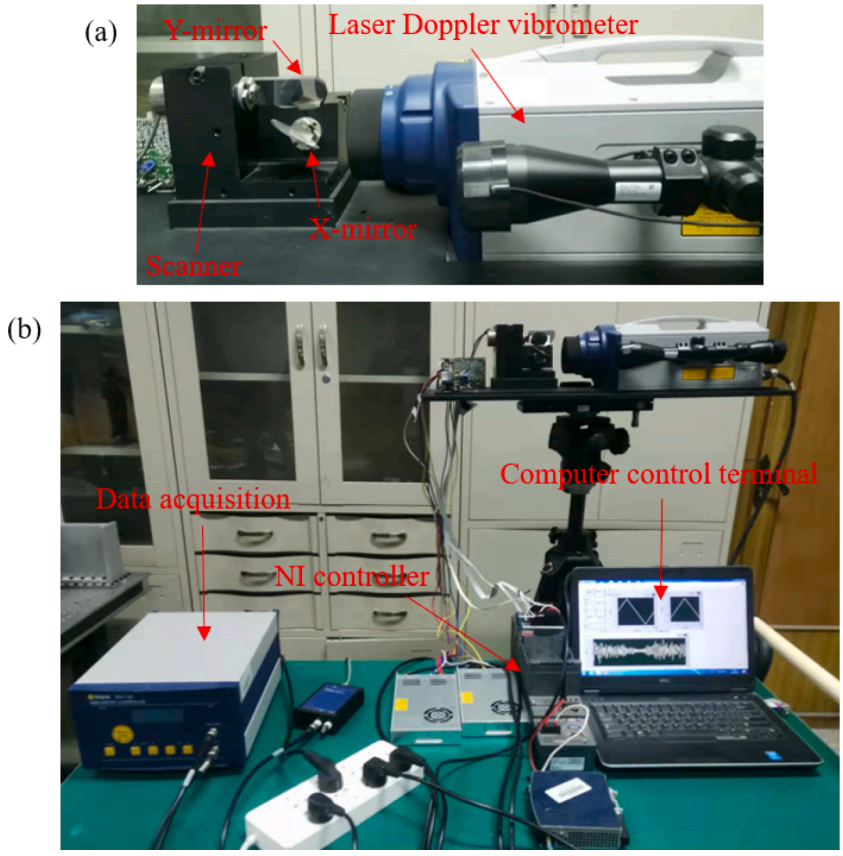

Fig. 10. Pictures of (a) the LCSLDV system for long-range measurement and (b) the experimental setup.

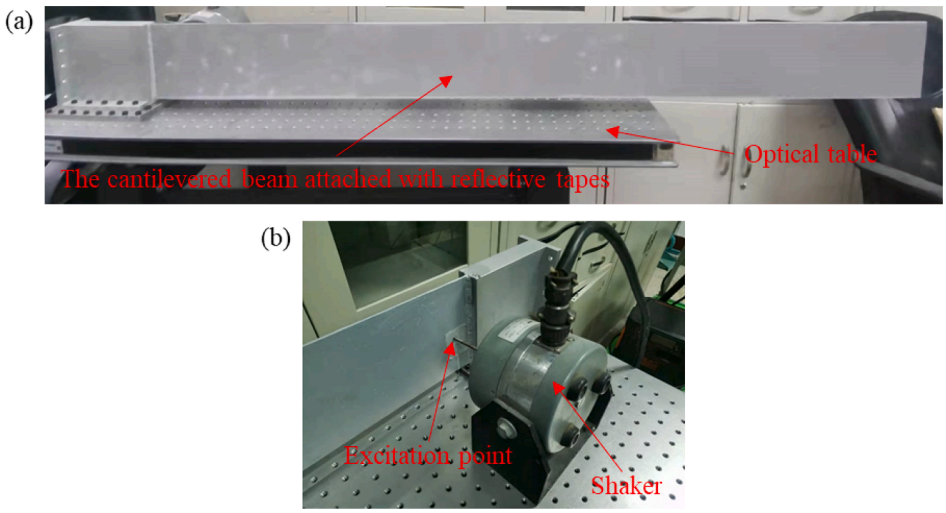

Fig. 11. Pictures of (a) the cantilever beam and (b) the shaker.

respectively. After that, $\boldsymbol{\phi}_I^r(x_l)$ and $\boldsymbol{\phi}_Q^r(x_l)$ can be obtained by multiplying corresponding filtered signals by two. During the estimation process of MSs, one of $\boldsymbol{\phi}_I^r(x_l)$ and $\boldsymbol{\phi}_Q^r(x_l)$ is the real part of the rth MS, and the other one is the imaginary part of that. The real parts of MSs are objects to be estimated, which completes the demodulation method.

4. Experimental investigation

4.1. Experimental setup

The bimodal interference phenomenon only evidently appears when the scanning length is more than 0.5 m. Considering that the maximum excitation force of the shaker in the laboratory was 50 N. Therefore, a cantilever beam with a length of 1500 mm, a width of 150 mm and a thickness of 3 mm was designed to verify the effectiveness and accuracy of the system [24,25]. The cantilever beam was machined according to the designed natural frequencies. In this way, the reliability of the LCSLDV system can be verified by comparing the calculated natural frequency with the measured natural frequency.

The LCSLDV system was developed in this work for measuring vibration of a distant structure, as shown in Fig. 10. The LCSLDV system includes a Polytec RSV-150 laser Doppler vibrometer, a Cambridge 6240H scanner with an NI 9082 controller and an outdoor power supply. The scanner was connected to the controller to control rotation angles of two orthogonal mirrors (X- and Y-mirrors) of the scanner. Since the laser beam of the vibrometer was reflected by the mirrors, horizontal and vertical positions of the laser spot on the structure could be controlled by changing rotation angles of the two mirrors, respectively. The laser Doppler vibrometer emitted a laser beam and it could measure the surface velocity of a point on the cantilever beam where the laser spot was located. The X- and Y-mirrors reflected the laser beam so that the laser beam was pointed at the long-range surface of the cantilever beam. A control scheme was programmed in a commercial software LabVIEW so that various scan paths of the laser spot could be designed by sending control signals to the scanner. The Y-mirror was fixed and the laser spot moved on the surface of the cantilever beam from one end of the scan path to its other end with the rotation of the X-mirror. Since the cantilever beam was sufficiently far away from the LCSLDV system and the rotation angle of the X-mirror was sufficiently small, horizontal and vertical positions of the laser spot could be considered to be linearly related to rotation angle of the X-mirror, respectively [26]. The feedback signal of the scanner that was registered in the form of voltage was used to indicate the rotation angle of the X-mirror.

This experiment was set up to estimate modal parameters and MSs of the designed cantilever beam using the OMA method described in Sec 3.1. The distance between the LCSLDV system and the scanned cantilever beam was 60 m. The shaker excites the cantilever beam at the cantilever end and a strip of a reflective tape was attached to the surface of the cantilever beam to enhance the signal-to-noise ratio of long-range measurement, as shown in Fig. 11. The scan path ranged from $x_l/L = 0$ to $x_l/L = 1$, as shown in Fig. 4, where x was the distance between the laser spot and the end point of the scan path close to the rotation center,

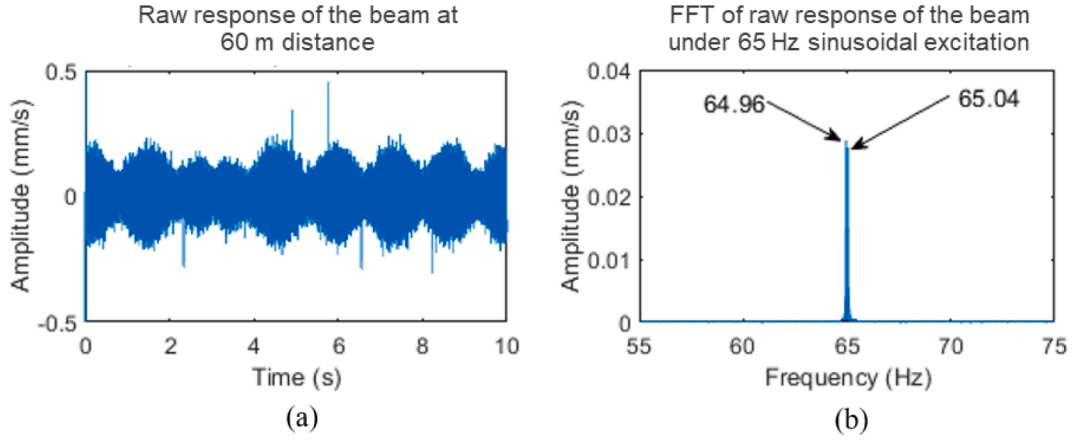

Fig. 12. (a) The raw response of the cantilever beam under 65 Hz sinusoidal excitation and (b) its spectrum.

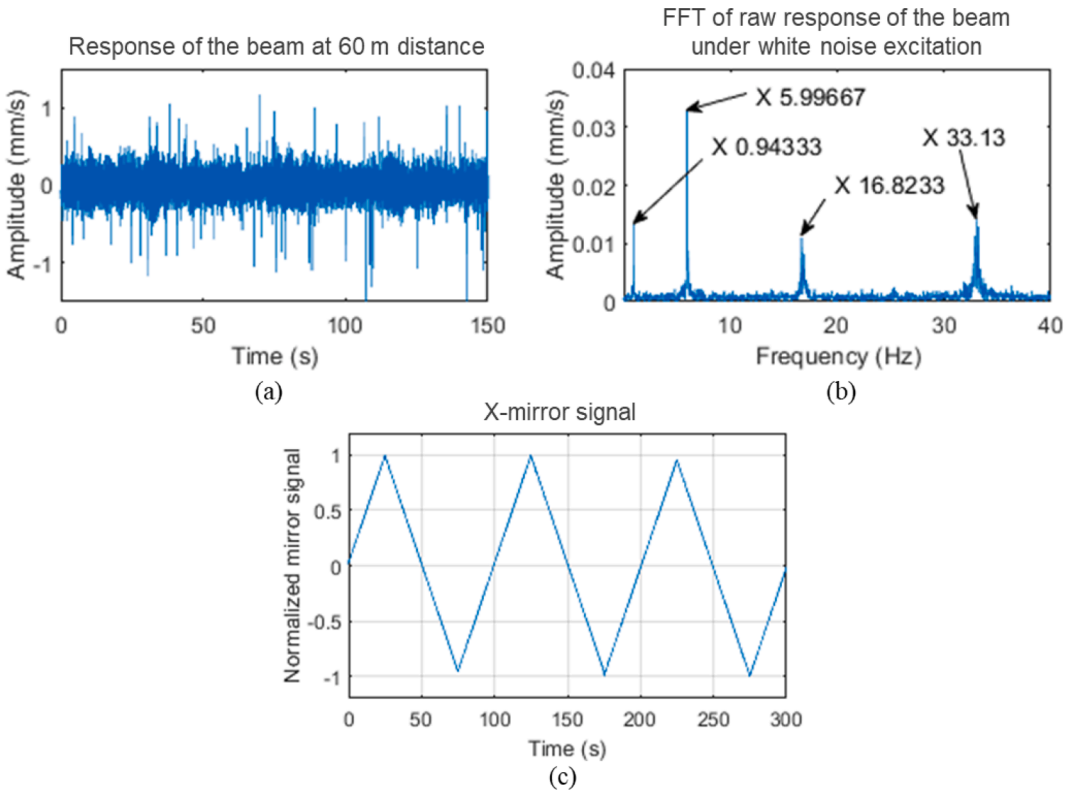

Fig. 13. (a) The raw response of the cantilever beam under white noise excitation, (b) itsspectrum and (c) the signal of the X-mirror.

and L was the length of the scan path.

4.2. Optimized OMA results

First, before the white noise excitation measurement, the cantilever beam was excited by sinusoidal excitation to check whether the system has eliminated bimodal interference. Control parameters of the LCSLDV system were set as follows: the scanning frequency of the X-mirror was 0.01 Hz and the sampling frequency was 1 k Hz. The distance between the measured cantilever beam and the LCSLDV system was 60 m and the speed of the laser spot sweeping on the surface of the cantilever beam was around 30 cm per second. As shown in Fig. 12, the raw response of the excited cantilever beam had some high amplitude time domain noises. However, in the spectrum, these noises had no effect on frequency recognition. It was obvious to identify that the accurate 65 Hz response measured by the LCSLDV system from the cantilever beam under a 65 Hz sinusoidal excitation, without any bimodal interference. Therefore, one can be sure that the measurement results of control parameters of the LCSLDV system were accurate and correct in the long-range measurement at a distance of 60 m.

Second, after determining that the LCSLDV system was accurate, the shaker generated white noise excitation to excite the cantilever beam. The LCSLDV system was located directly in front of the geometric center of the cantilever beam so that the LCSLDV system could measure the transverse vibration of the cantilever beam and the raw response could be processes to estimate modal parameters of cantilever beam bending modes. The control parameters of the LCSLDV system were the same in the whole measurement. The LCSLDV system measurement was performed to estimate the MSs of the cantilever beam. Because bimodal interference caused by the scanning frequency coupling was eliminated, dominant frequencies in the spectrum after the FFT were very legible and could be accurately identified, although there were other interference signals in the measured response. As shown in Fig. 13, dominant frequencies of the first four natural frequencies of the cantilever beam in the spectrum were measured. The first cantilever beam bending mode was identified at 0.94333 Hz and the mode at 5.99667 Hz was found to be the second bending mode of the cantilever beam. The value of the third and fourth frequencies were 16.8233 Hz and 33.13 Hz, respectively.

Then, for every bending mode of the cantilever beam, the raw response measured by the LCSDLV system was processed with a band-pass filter centered on the frequency of the mode to be derived. The demodulation method described in **Sec 3.1** was implemented to the filtered response to extract the MSs of the cantilever beam. As shown in Fig. 14, the normalized MSs of the first four modes of the cantilever beam were obtained from the demodulation method. In addition, the first four MSs obtained by the FEM were also shown in Fig. 14 for comparison purposes. The formation ends of MSs flatted out as a result of filtering during the demodulation method used in the LCSLDV measurement.

Modal assurance criterion (MAC) values are calculated as the normalized scalar product of the two sets of MSs $\boldsymbol{\phi}_A$ and $\boldsymbol{\phi}_X$ [27]. They are arranged into the MAC matrix

$$MAC(r,q) = \frac{\left|\{\boldsymbol{\phi}_A^r\}^T\{\boldsymbol{\phi}_X^q\}^T\right|}{\left(\{\boldsymbol{\phi}_A^r\}^T\boldsymbol{\phi}_A^r\right)\left(\{\boldsymbol{\phi}_X^q\}^T\boldsymbol{\phi}_X^q\right)} \tag{27}$$

where $\boldsymbol{\phi}_A^r$ is the MS vector of the rth mode from the LCSLDV measurement, $\boldsymbol{\phi}_X^q$ is the MS vector of the qth mode from the FEM and T is the transpose of a matrix. The values of the diagonal components in the MAC matrix extracted from the LCSLDV measurement and the FEM were illustrated in Table 2 and the MAC matrix was demonstrated in Fig. 15.

It can be seen from Table 2 that the natural frequencies obtained by the FFT of the raw response measured by the LCSLDV system was basically consistent with them obtained by finite element simulation. Let r_1 be the relative error of the values of the natural frequencies from the FEM and the LCSLDV system. The maximum deviation of natural frequencies from the FEM and the LCSLDV system was 2.97% and the

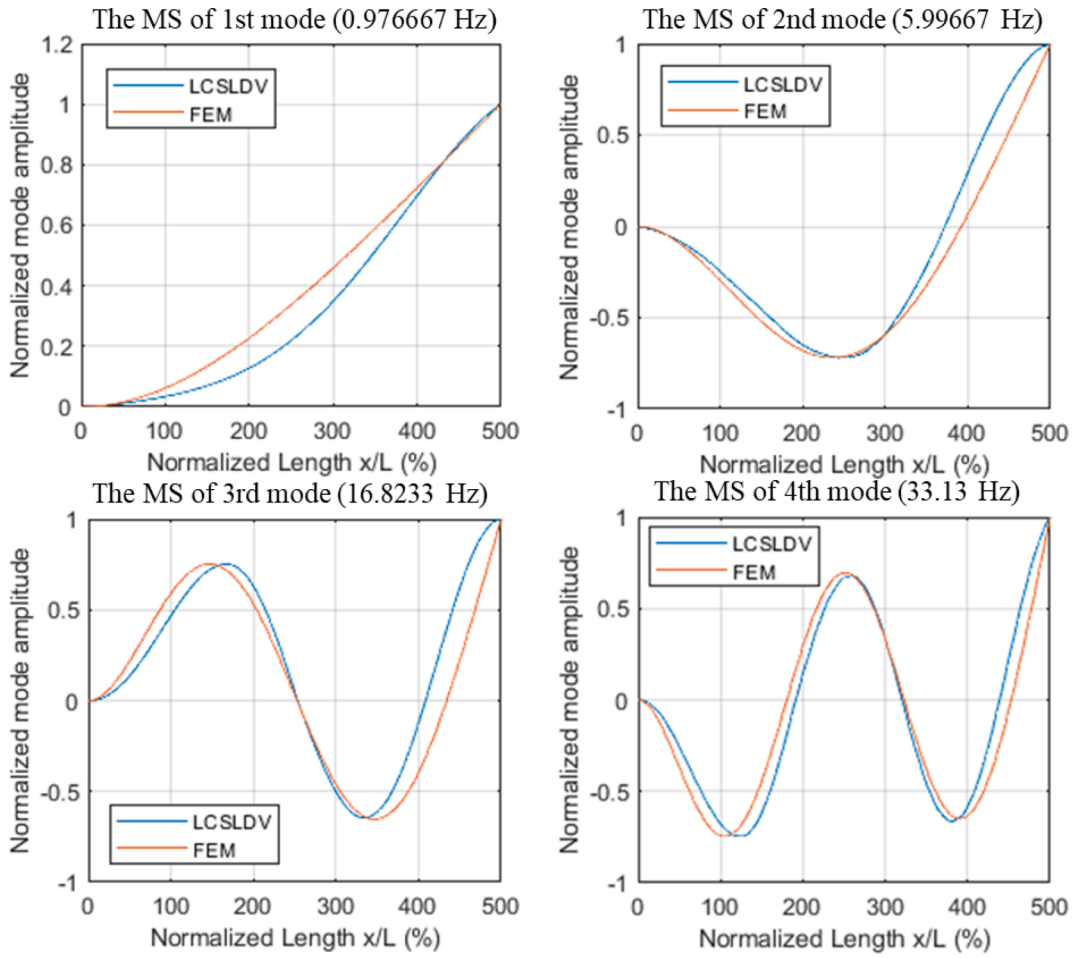

Fig. 14. The MSs of the first four modes of the cantilever beam.

Table 2
Comparison of the natural frequencies from the FEM and the LCSLDV system.

Mode	FEM	LCSLDV	r_1	MAC
1	0.97144 Hz	0.94333 Hz	2.97%	0.98420
2	6.0861 Hz	5.99667 Hz	1.49%	0.95282
3	17.053 Hz	16.8233 Hz	1.36%	0.92304
4	33.466 Hz	33.13 Hz	1.1%	0.93578

minimum deviation was 1.1%. The deviation of this magnitude was unavoidable because there were machining error and the clamped boundary condition of the cantilever beam could not be an ideal boundary condition. Note that it was acceptable that the MAC value of the fourth mode was 0.92304 since the flattening of the end of the MSs caused by filtering was inevitable [28].

5. Conclusion

This paper introduced the cause and the elimination of interference caused by signal coupling of the scanning frequency and vibration frequencies in the spectrum, which was ignored by most LCSLDV measurements. This kind of interference signal was named bimodal interference in this paper because it caused two symmetrically shifted peaks centered at the dominant frequency in the spectrum, making it impossible to determine the precise value of the dominant frequency. The frequency shift of bimodal interference was positively correlated with the scanning frequency of the mirror. The trigonometric functions from the perspectives of optics and dynamics and discretized by time

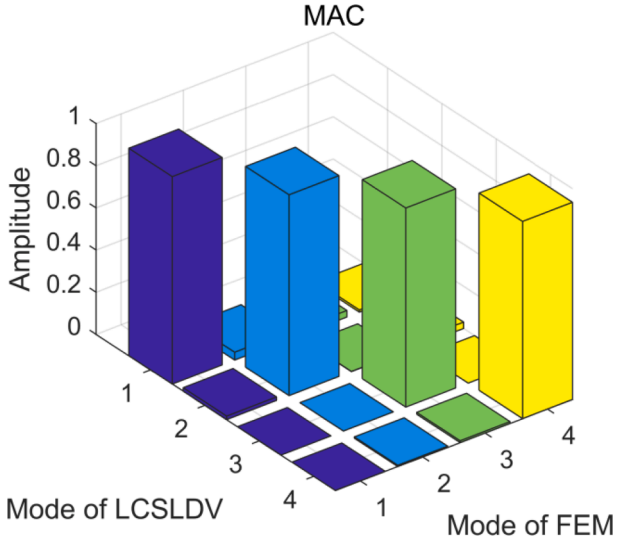

Fig. 15. MAC matrix extracted from the LCSLDV system and the FEM.

series were used to represent the laser spot reflected from the X-mirror and going to the cantilever beam. Through analyzing the trigonometric functions of the incidence and reflection of the laser beam with continuous scanning in a tiny time interval, the mathematical explanation of the symmetric frequency shifts centered at the dominant frequency caused by the scanning frequency was derived. By analyzing

Fig. 16. Pictures of (a) classical modal measurement of the cantilever beam and (b) the layout of the accelerometer.

Table 3
Comparison of the natural frequencies measured by the traditional modal analysis method and the LCSLDV system.

Mode	SMM	LCSLDV	r_2
1	0.9506 Hz	0.94333 Hz	0.77%
2	5.9422 Hz	5.99667 Hz	−0.91%
3	16.6968 Hz	16.8233 Hz	−0.75%
4	32.8925 Hz	33.13 Hz	−0.72%

mathematical equations, it can be known that when the scanning frequency increases, the value of the frequency shift caused by bimodal interference increases simultaneously. The effect of bimodal interference is too obvious to ignore in LCSLDV measurement.

The experimental results of nine groups with different sampling frequencies illustrated that there was no aliasing in the system and bimodal interference was independent of the sampling frequency under the insurance of the sampling accuracy. The experimental results of six groups with different measuring distances demonstrated that the frequency shifts of bimodal interference would not decrease with the decrease of the measuring distance in long-range measurement. The experimental results of six groups with different scanning frequencies illustrated that the frequency shifts of bimodal interference would not decrease with the decrease of the measuring distance in long-range measurement. The experimental results of six groups of scanning frequencies demonstrated that the symmetric frequency shifts of the dominant frequency in long-range measurement was caused by the scanning frequency of the mirror. There was a positive correlation between the scanning frequency and the value of symmetric frequency shifts of the dominant frequency in the spectrum caused by bimodal interference. The phenomenon of bimodal interference was inconspicuous if the scanning length was less than 0.5 m. When the scanning frequency was reduced to 0.01 Hz, bimodal interference in the spectrum of the raw response from the LCSLDV measurement at 60 m almost disappeared because the value of the symmetric frequency shifts was 3 orders of magnitude lower than the dominant frequency.

This work also reported the first long-range continuously scanning measurement with Polytec RSV-150 laser Doppler vibrometer. It is significant to recode accurate results without bimodal interference in LCSLDV measurement. From this, natural frequencies in long-range continuously scanning measurement can be accurately estimated. Due to ambient noise, the interference signal in the raw response of long-range measurement is inevitable, the optimized OMA results in this paper shows that it hardly affects modal parameter estimation of the LCSLDV system.

CRediT authorship contribution statement

Yuhao Hu: Conceptualization, Methodology, Validation, Formal analysis, Investigation, Data curation, Writing – original draft. **Weidong Zhu:** Conceptualization, Methodology, Writing – review & editing, Funding acquisition, Supervision, Project administration. **Linfeng Lyu:** Methodology, Software. **Zhonggang Li:** Funding acquisition, Resources, Supervision, Project administration.

Declaration of Competing Interest

The authors declare that they have no known competing financial interests or personal relationships that could have appeared to influence the work reported in this paper.

Data availability

Data will be available on request.

Acknowledgement

The authors are grateful for the financial support from the National Natural Science Foundation of China (No. 11772100) and National Key Research and Development Program of China (No. 2019YFE013200). The authors would like to thank Xi Chen for some valuable discussion on the LCSLDV system.

Appendix:. Traditional modal analysis results for the cantilever beam

In order to verify the accuracy of the modal parameters of the cantilever beam excited by the shaker at the cantilever end, a classical modal measurement was implemented on the cantilever beam as shown in Fig. 16. An acceleration was attached at the position with 10 cm from the free end of the cantilever beam. Fifteen points were evenly spaced on the central axis of the cantilever beam. The distance between each point was 10 cm. The first four natural frequencies of the cantilever beam, which were illustrated in Table 3, were analyzed by the m + p software after fifteen points were hit by an impact hammer. One can know that the maximum deviation of the natural frequencies measured by the traditional modal analysis method and the LCSLDV system was 0.91%. Let r_2 be the relative error of the value of the natural frequencies measured by the traditional modal analysis method and the LCSLDV system, and the normalized standard deviation of r_2 was 0.007861. The traditional modal analysis method is the most basic and reliable modal measurement method. Hence, such a small deviation indicates that the natural frequencies of the cantilever beam measured by the LCSLDV system were accurate.

References

[1] J.R. Bell, S.J. Rothberg, Laser vibrometers and contacting transducers, target rotation and six degree-of-freedom vibration: what do we really measure? J. Sound Vib. 237 (2000) 245–261.

[2] Y. Yeh, H.Z. Cummins, Localized Fluid Flow Measurements with an He-Ne Laser Spectrometer, Appl. Phys. Left. 4 (10) (1964) 176–178.

[3] R. Huang, X.M. Nie, J. Zhou, Laser Doppler velocimeter and its calibration system, Measurement 134 (2019) 286–292.

[4] J. Zhou, X.W. Long, A novel mathematic model of LASER Doppler velocimeter for the velocity measurement of solid-state surface, Measurement 45 (1) (2012) 14–18.

[5] A.B. Stanbridge, D.J. Ewins, Modal testing using a scanning laser doppler vibrometer, Mech. Syst. Signal Pr. 13 (2) (1999) 255–270.

[6] P. Sriram, S. Hanagud, J. Craig, N.M. Komerath, Scanning laser Doppler technique for velocity profile sensing on a moving surface, Appl. Opt. 29 (16) (1990) 2409–2417.

[7] P. Hariharan, B. Ward, Interferometry and the Doppler effect an experimental verification, Optica. Acta: Int. J. Optics. 44 (2) (1997) 221–223.

[8] M. Martarelli, D.J. Ewins, Continuous scanning laser Doppler vibrometry and speckle noise occurrence, Mech. Syst. Signal Pr. 20 (8) (2006) 2277–2289.

[9] D. Di Maio, P. Castellini, M. Martarelli, S. Rothberg, M.S. Allen, W.D. Zhu, D. J. Ewins, Continuous Scanning Laser Vibrometry: A raison d'ètre and applications to vibration measurements, Mech. Syst. Signal Pr. 156 (12) (2021), 107573.

[10] P. Sririam, S. Hanagud, J.I. Craig, Mode shape Measurement Using a Scanning Laser Doppler Vibrometer, Int. J. Anal. Exp. Modal Anal. 7 (3) (1992) 169–178.

[11] A.B. Stanbridge, D.J. Ewins, Using a Continuously-Scanning Laser Doppler Vibrometer for Modal Testing, 14th Int. Modal Analysis Conference (IMAC), Dearborn, MI, Feb.12–15 (1996) 816–822.

[12] A.B. Stanbridge, A.Z. Khan, D.J. Ewins, Modal testing using impact excitation and a scanning LDV, Shock Vib. 7 (2) (2000) 91–100.

[13] D. Di Maio, D.J. Ewins, Continuous Scan, a method for performing modal testing using meaningful measurement parameters Part I, Mech. Syst. Signal Pr. 25 (8) (2011) 3027–3042.

[14] D.M. Chen, Y.F. Xu, W.D. Zhu, Damage Identification of Beams Using a Continuously Scanning Laser Doppler Vibrometer System, J. Vib. Acoust. 138 (5) (2016), 051011.

[15] L.F. Lyu, W.D. Zhu, Operational modal analysis of a rotating structure subject to random excitation using a tracking continuously scanning laser Doppler vibrometer via an improved demodulation method, J. Vib. Acoust. 144 (1) (2022), 011006.

[16] S. Yang, M.S. Allen, Lifting approach to simplify output-only continuous-scan laser vibrometry, Mech. Syst. Signal Pr. 45 (2) (2014) 267–282.

[17] J.L. Feinberg, A. Rebane, Method of imaging through a scattering medium using coherent light, US (1994) 5313315.

[18] T. Lv, X. Han, S. Wu, Y. Li, The effect of speckles noise on the Laser Doppler Vibrometry for remote speech detection, Optics Commun. 440 (2019) 117–125.

[19] G. Jin, Z.L. Li, Eliminating Speckle Noises for Laser Doppler Vibrometer Based on Empirical Wavelet Transform, in: 13th International Conference on Measurement, 2021, https://doi.org/10.23919/Measurement52780.2021.9446777.

[20] D.W. Beran, B.C. Willmarth, F.C. Carsey, F.F. Hall, An acoustic Doppler wind measuring system, J. Vib. Acoust. 55 (2) (1974) 334–338.

[21] Y. Hu, Y. Kang, K. Yu, W. Zhu, R. Zhao, Complete operating deflection shapes and model updating for an excited structure in thermal environments via an optimized continuously scanning laser Doppler vibrometer with a two-dimension scan scheme, J. Sound Vib. 544 (2023) 117411.

[22] A.P. Song, Study of Continuously Scanning Laser Doppler Vibrometer Test and Modal Analysis Technique, Master's dissertation, NUAA, 2017.

[23] B.J. Halkon, S.J. Rothberg, Vibration measurements using continuous scanning laser Doppler vibrometry: theoretical velocity sensitivity analysis with applications, Meas. Sci. Technol. 14 (3) (2003) 382.

[24] K.P. Yu, J.X. Zou, Struct. Dyn, 3rd Edition,, Harbin Institute of Technology Press, 2015.

[25] W.D. Qu, H.L. Tang, Mech. Vib. Manual -, 2nd edition,, China Machine Press, 2000.

[26] Y.F. Xu, D.M. Chen, W.D. Zhu, Operational modal analysis using lifted continuously scanning laser Doppler vibrometer measurements and its application to baseline-free structural damage identification, J. Vib. Control. 25 (7) (2019) 1341–1364.

[27] M. Pastor, M. Binda, T. Hararik, Modal Assurance Criterion, Procedia Eng. 48 (2012) 543–548.

[28] P. Avitabile, Modal space - in our own little world, Exp. Tech. 38 (4) (2005) 3–5.